Rocznik Ochrona Środowiska
Volume 27 Year 2025 ISSN 2720-7501 pp. 174-195
https://doi.org/10.54740/ros.2025.015 open access
Received: September 2024 Accepted: March 2025 Published: April 2025

Structural Response of Beam-Column Joint Made of Fiber Reinforced Concrete (FRC) Using ANSYS FEA Simulation

Isha Verma[1], Lalit Gautam[2], Shruti Gomkale[3], Anuj Goyal[4], Parveen Berwal[5], Abdullah Faiz Al Asmari[6], Saiful Islam[7]*
[1]*Civil Engineering Department, MDU-UIET, Rohtak, India*
[2]*Research Scholar, Civil Engineering Department, MDU-UIET, Rohtak, India*
[3]*Department of Applied Chemistry, Yeshwantrao Chavan College of Engineering, Nagpur, India*
[4]*Civil Engineering Department, GLA University, Mathura, India*
https://orcid.org/0000-0002-5371-6323
[5]*Civil Engineering Department, Galgotias College of Engineering & Technology, Greater Noida, India*
https://orcid.org/0000-0003-2422-3391
[6]*Civil Engineering Department, College of Engineering, King Khalid University, Abha, Saudi Arabia*
[7]*Civil Engineering Department, College of Engineering, King Khalid University, Abha, Saudi Arabia*

[*]*corresponding author's e-mail: isha.1272@gmail.com*

Abstract: Beam-column joints are crucial in reinforced concrete and steel structures, which transfer load from beams to columns and vice versa. They are essential to withstand various types of loads, such as lateral, gravity, and seismic loads. The material of the beam-column joint determines the joint's ability to withstand and transfer loads between beams and columns. The stronger material would enhance its strength and overall load-bearing capacity and vice versa. Current research aims to evaluate the structural response of beam-column joints made of Fiber Reinforced Concrete (FRC's) using ANSYS FEA simulation package. The effect of fiber concentration, i.e., 0.3%, 0.6%, and 0.9%, on the strength of the beam-column joint is evaluated based on structural evaluation parameters. The other objective is to evaluate the effect of graphene fiber (the aspect ratio is 1:1, although up to 1.5 is typically acceptable) on improving the strength of the beam-column joint. Comparative studies are conducted, and materials are evaluated based on stiffness, ductility and energy dissipation. The graphene-reinforced concrete demonstrates less stiffness degradation with increased strain. This indicates that the incorporation of graphene improves the stiffness retention capacity of the concrete. The hysteresis loop of graphene-reinforced concrete is broader, signifying enhanced ductility. This indicates that the material can sustain greater deformations without failure, essential for seismic performance. The 0% FRC has minimal ductility, characterized by a notable reduction in stress upon first loading. The 0.3% and 0.6% FRC show improved ductility, with higher stress levels maintained over larger strains. The 0.9% FRC demonstrates the highest ductility, maintaining higher stress over the full strain range, indicating it can undergo larger deformations without failure. The stiffness degradation is less pronounced in higher FRC concentrations.

Keywords: beam, column, steel structure, reinforced concrete, graphene

1. Introduction

Beam-column joints are critical regions where beams and columns intersect in reinforced concrete (RC) and steel frame structures. These joints play a crucial role in transferring loads between beams and columns and ensuring the overall stability and integrity of the structure, especially under seismic loading conditions (Mahmoud et al. 2020, Zoubek et al. 2013). The beam-column joints are significant in enhancing the overall stability and integrity of concrete structures. The beam-column joints are highly vulnerable to failure at dynamic loads (seismic excitations) with high shear forces, bending moments, and axial loads (Wang et al. 2018, Batalha et al. 2022). Due to the high magnitude of induced stresses at seismic excitation, the structure bears catastrophic structural damage, and thereby, it demands good reinforcement strategies (Dang & Dinh 2017).

The conventional concrete material requires reinforcement to enhance its durability and tensile strength. The FRC's incorporating fibers offers a good solution to improve the mechanical properties of concrete (del Vecchio et al. 2015, del Vecchio et al. 2016, Cimmino et al. 2020). The fiber concentration in FRC's significantly affects the mechanical properties of concrete. The optimal fiber concentration in FRC's is required to attain good beam-column joint strength. There is a lack of comprehensive data on using FRC's for beam-column joints. The fiber concentrations in FRC (0.3%, 0.6%, and 0.9%) have a significant effect on the structural response of beam-column joints subjected to repetitive cyclic or dynamic loads (earthquake), which are not addressed (Guan et al. 2016, Wahjudi et al. 2014, Dimov et al. 2018). The effect of fiber concentration of FRC's on stiffness, ductility, and energy dissipation capacity of beam-column joints is not addressed, which limits the ability to optimize FRC compositions for our beam-column joint applications (Ilia & Mostofinejad 2019). The conventional methods used to study the beam-column joint employed experimental testing methods that are expensive and time-consuming. There is a need to develop a numerical model for the evaluation of the beam-column joint, which can be later used for optimizing the design parameters of the beam-column joint as well as other properties of the material (Santarsiero & Masi 2015, Wang et al. 2019, Parra-Montesinos et al. 2005).

1.1. Functional Requirement of Beam-Column Joint

The functional requirements for the beam-column connection are an important concern in structural engineering (Ghayeb et al. 2020). It refers to specific performance criteria the combination must achieve to maintain the structure's overall stability and integrity. The functional requirements of the beam-column connection are typically dictated by parameters such as load transfer, stiffness, strength, and durability (Behnam et al. 2017, Waqas et al. 2023). The junction, also known as the intersection of beams and columns, is designed to allow for the maximum extension and maintenance of nearby elements.

The connectors must possess adequate rigidity and strength to endure the internal stresses generated by the framework components (Waqas et al. 2024, Wang et al. 2020, Ghayeb et al. 2017). The prerequisites for achieving optimal joint function can be clearly defined as follows:

1. The strength of the joint must meet or surpass the most rigorous criterion related to the formation of the structural plastic hinge mechanism for the frame. The elimination of the need for combined processes to distribute energy and restore power in a challenging region would be achieved. It will be subsequently shown that joint mechanisms undergo a significant reduction in rigidity and strength when exposed to cyclic operations within the inelastic range (Jian-Qiang & Yang 2013, Isha Verma & Setia 2019, Isha Verma et al. 2020).
2. The capacity of the column to bear weight should not be affected by any potential decrease in joint strength. The column is considered incomplete if the joint is not present.
3. Including unnecessary joint reinforcement, which does not contribute to achieving optimal performance, should not add complexity to the construction process.

1.2. Beam-Column Joint Failure

Following the occurrence of the earthquake, subsequent inspections have indicated that the structures were rendered in a state of destruction due to inadequate adherence to construction protocols. Some residential and corporate structures were built without adequate measures to ensure earthquake resistance (Kremmyda et al. 2017, Megget 2003). The structural failures observed in the earthquake-affected region can be attributed to a combination of various factors. The structural issues of the building can be attributed to several factors (Kosior-Kazberuka et al. 2016).

The inadequate strength of beam-column connections negatively impacts the seismic performance of structures built with reinforced concrete (RC). The presence of structures that have suffered significant damage or complete destruction within the seismic zone serves as evidence for this phenomenon (Magliulo et al. 2017, Khan et al. 2018, Algassem & Vollum 2023). Figure 1 shows the damage incurred on the Joints of a building.

Fig. 1. Damage incurred on Joints

2. Historical Background

Since the inception of human civilization, beam-column joints can be traced back to ancient Egyptian and Mesopotamia in 3000 B.C. Various architectures and temples of this era employed stone columns supporting beams. However, these beam columns were simple post and lintel systems without sophisticated joints. Greek and Roman architecture also portrays the application of refined beam column joints made of stone and marble. They have built large buildings like basilicas and aqueducts incorporating beam-column joints and demonstrated a good understanding of load transfer and structural stability.

Ghayeb et al., The main objective of the experimental and analytical research is to study the behavior of concrete beam-column junctions that utilize high-yield strength bars in both the beams and columns. The design requirements for high-strength steel reinforcements in ACI 318 and NZS 3101 are evaluated to determine their validity. The bond conditions of the specimens have been shown to be improved through the implementation of axial compression loading and the utilization of high-strength concrete. The tests conducted are as per the schematic shown in Figure 2. The findings of this examination suggested that every specimen displayed symptoms characteristic of a ductile failure mechanism. The energy dissipation capacity was diminished through the implementation of High-Strength Steel (HSS) reinforcements, whereas the energy dissipation was significantly augmented through the utilization of axial compression tension. Implementing longitudinal beam reinforcements with a higher grade led to a marginal decrease in bond strength within the joint area (Parveen Berwal et al. 2024).

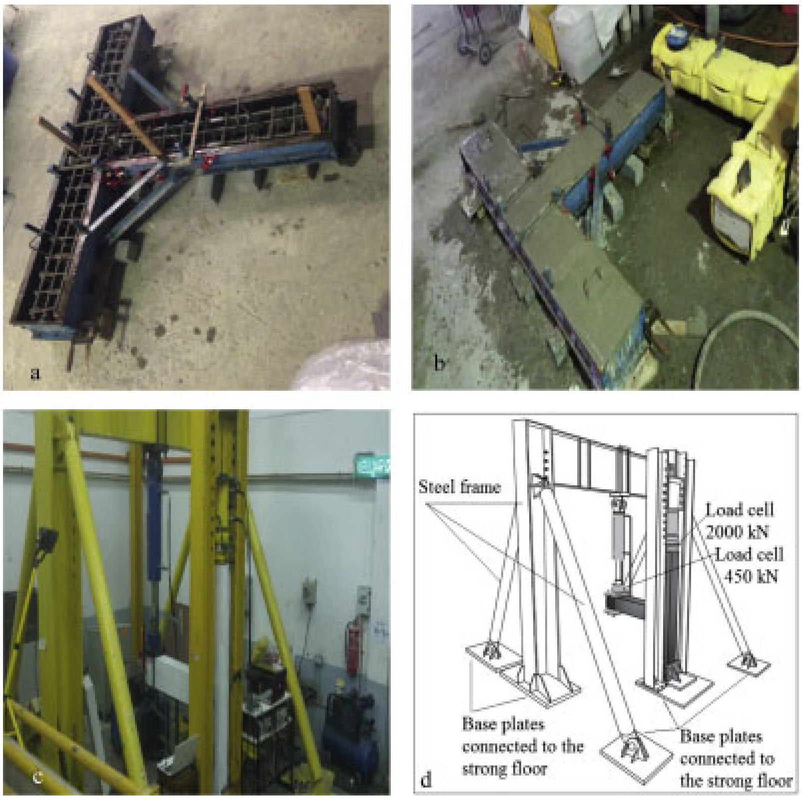

Fig. 2. View of the RC series for: (a) steel mold and reinforcement, (b) casted RC model sample, (c) RC model test setup, and (d) schematic diagram of the test setup for the exterior connections

Tsang et al. investigated the usage of sheathed bars to enhance the seismic performance of external joints. Their research, published in the ACI Structural Journal, revealed that encased bars enhance anchoring while decreasing reinforcement density in the joint region, leading to superior seismic performance. (Wang et al. 2019) investigated the utilization of composite sheaths for the seismic fortification of beam-column connectors. Their research, published in the Journal of Structural Engineering, indicated that composite sheaths can markedly enhance connections' shear capacity and ductility. They provided pragmatic guidance for employing composite materials in retrofit initiatives, highlighting the benefits of straightforward installation and longevity (Parveen Berwal et al. 2023, Realfonzo et al. 2014, Sharma & Bansal 2019).

(Wahjudi et al. 2014) The objective is to deliver an exhaustive comprehension of the link's hysteresis behavior. Applying the finite-element method is utilized to employ a mathematical model that incorporates the compression effect commonly observed in concrete structures. The model will be implemented numerically and modified using the computer code Seismic Struct once it has been established within a spring element. The load-deformation behavior of BCC is shown in Figure 3. A wide range of numerical data and calibrations are entered to create a detailed record of response history (Alavi-Dehkordi et al. 2019).

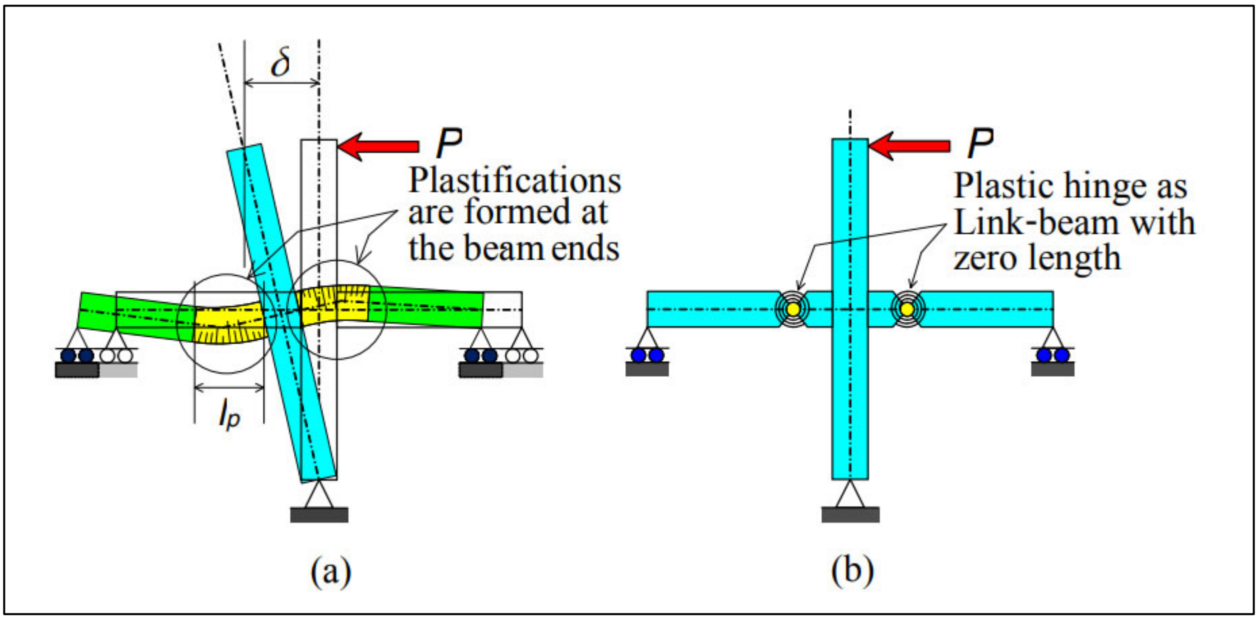

Fig. 3. The lead deformation behavior of BCC

(Ghayeb et al. 2020) studied how fiber-reinforced plastics affected the seismic performance of beam-column couplings. Their findings revealed the significant improvements in joint strength and ductility attained through FRP strengthening. They made specific recommendations for selecting and applying FRP materials in seismic retrofit projects.

The effect of vertical earthquake components on the performance of beam-column assemblies was evaluated by (Fawzia et al. 2021). Their research, which was published in Earthquake Engineering & Structural Dynamics, emphasized how important it is to consider vertical accelerations when designing in tandem. They proposed changes to the existing design specifications to take these impacts into account and provide a more thorough method of seismic engineering.

A thorough investigation was conducted on the collapse risk of decaying reinforced concrete structures with inadequate beam-column connections (Batalha et al. 2022). Their study, which was published in the Journal of Structural Engineering, revealed serious flaws in joint details that could cause devastating earthquakes. They suggested improvement tactics and design changes that would increase the safety of existing structures to lessen these risks.

The impact of bond shear behavior on the seismic response of beam-column connections was investigated by (Waqas et al. 2023). Their paper thoroughly examines bond slip processes and how they affect joint performance. It was published in the ACI Structural Journal. Bond slip behavior was predicted using models, which were then used to build and assess seismic applications. A computational model was created to mimic the cyclic behaviour of reinforced concrete beam-column connections. The model demonstrated the complex relationships that exist between reinforcement and concrete when there is seismic loading. His work has developed improved modeling tools for studying and designing seismically resilient structures.

3. CAD Modelling

The CAD model of the beam-column joint is developed in CAD design software. The schematic of the beam-column joint is shown in Figure 4. As per the schematic, the beam-column model is developed using sketch and extrude tools. Multiple copies of reinforcement and rebars are generated using the pattern tool, as shown in Figure 5.

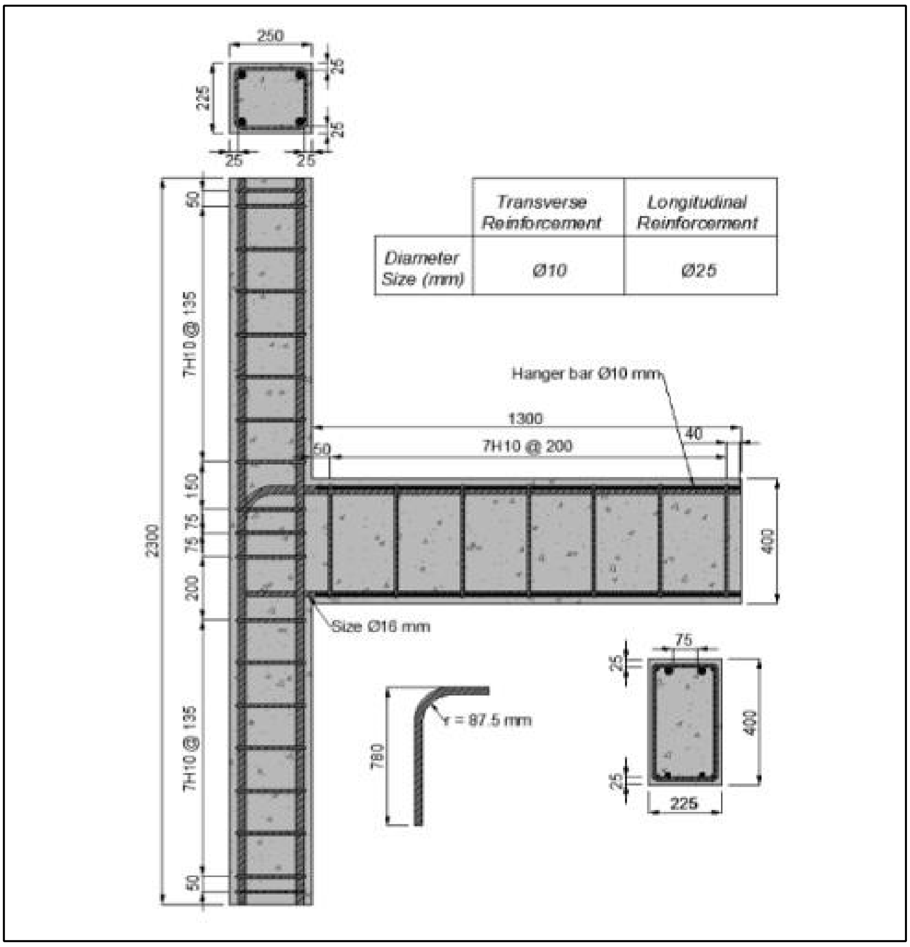

Fig. 4. Schematic of the beam-column joint with L bars (Batalha N, et al. 2022)

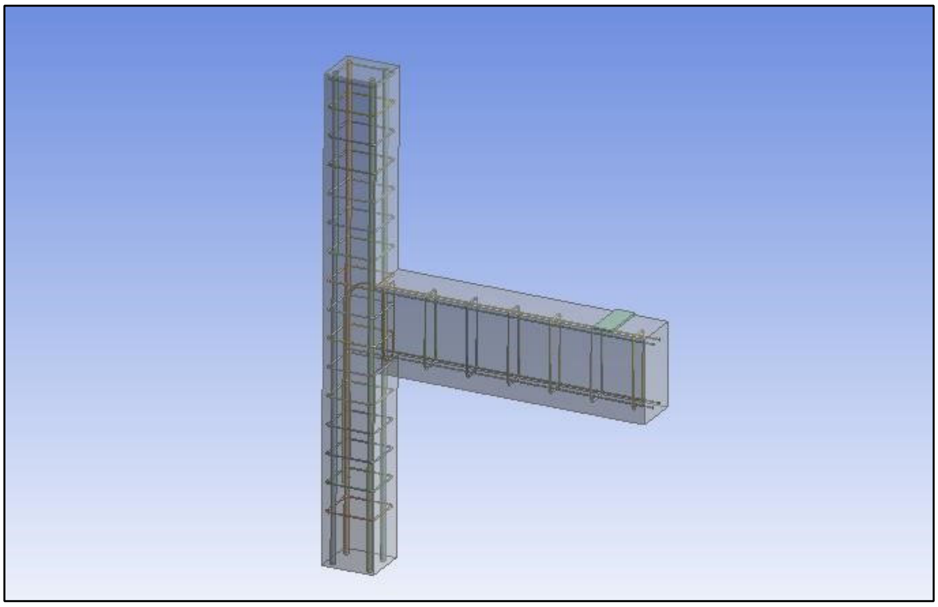

Fig. 5. CAD model of the beam-column joint with L bars

3.1. Meshing

After modeling, the beam-column design is meshed using tetrahedral element type, as shown in Figure 6. The discretization process involves setting up a transition ratio, with inflation set to normal and the growth rate set to 1.2. The size function for the beam-column geometry is set to adaptive type, and the relevance center is set to medium and fast transition.

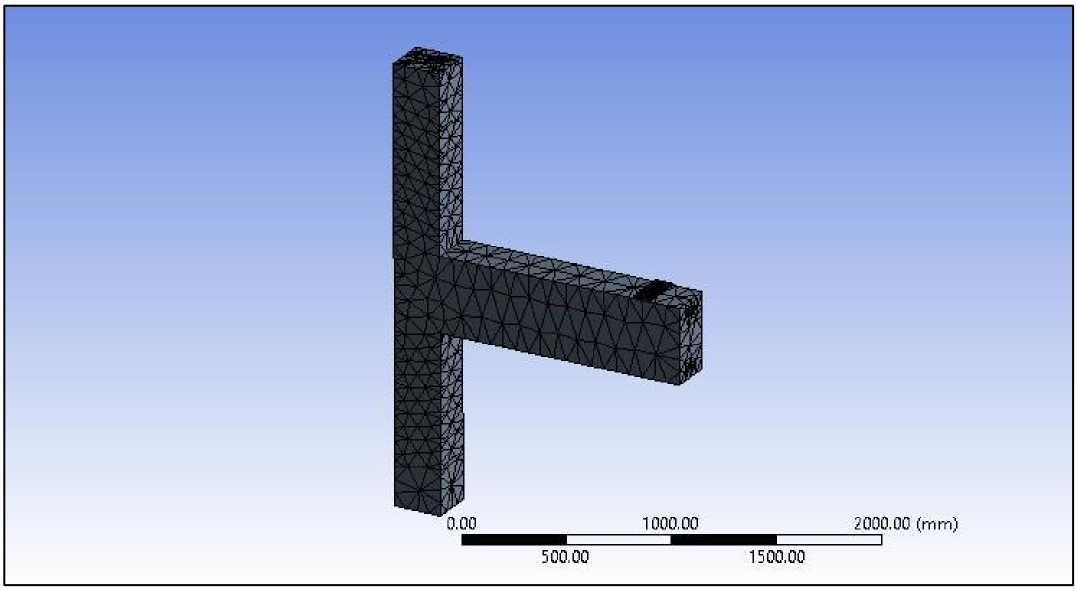

Fig. 6. Meshed model of the beam-column joint with L bars

3.2. Loading Conditions

After discretization, the structural boundary conditions are applied to the beam-column model, as shown in Figure 7. The column is applied with 300000 N, and the beam is applied with vertical loads in steps, as shown in Table 1.

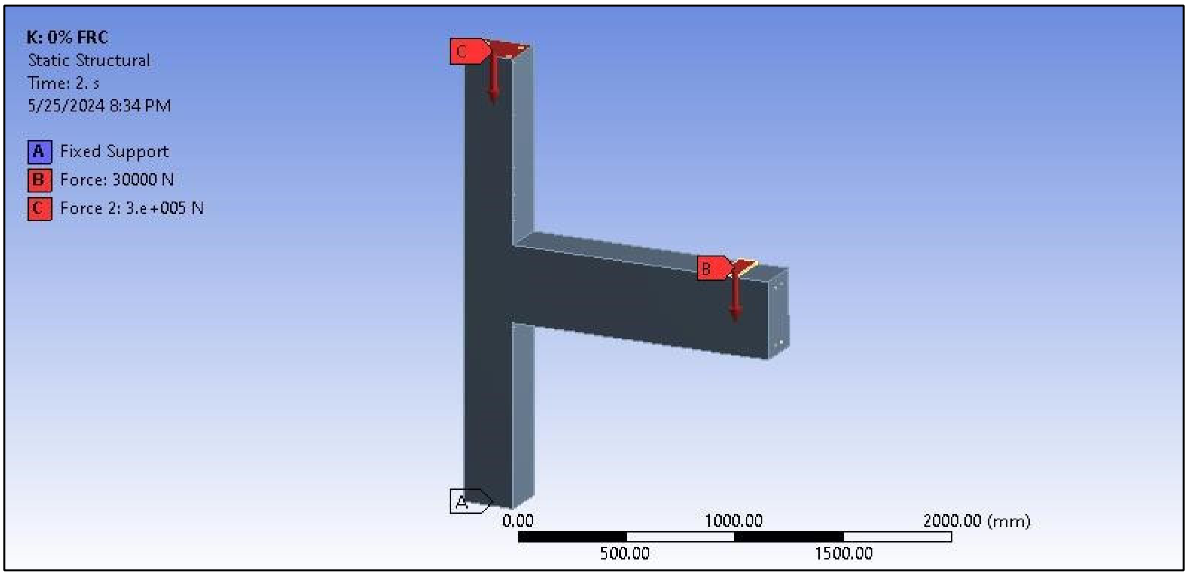

Fig. 7. Applied boundary conditions

Table 1. Applied loads on beams

Steps	X [N]	Y [N]	Z [N]
1	0	0	10000
2	0	0	20000
3	0	0	30000
4	0	0	40000
5	0	0	50000
6	0	0	60000
7	0	0	70000

Steps	X [N]	Y [N]	Z [N]
8	0	0	80000
9	0	0	90000
10	0	0	100000
11	0	0	110000
12	0	0	120000
13	0	0	130000

These loads are applied in different steps, starting from 10 kN in step 1 and reaching up to 130 kN in step 13.

3.3. Structural Analysis using 0% FRC Material

The beam-column joint's structural analysis is conducted using 0% FRC at different loads. The induced deformation on the beam-column joint at 40 kN load is shown in Figure 8. The maximum deformation magnitude is obtained at the beam end as represented by the red-colored zone, wherein the magnitude is obtained at 11.096 mm.

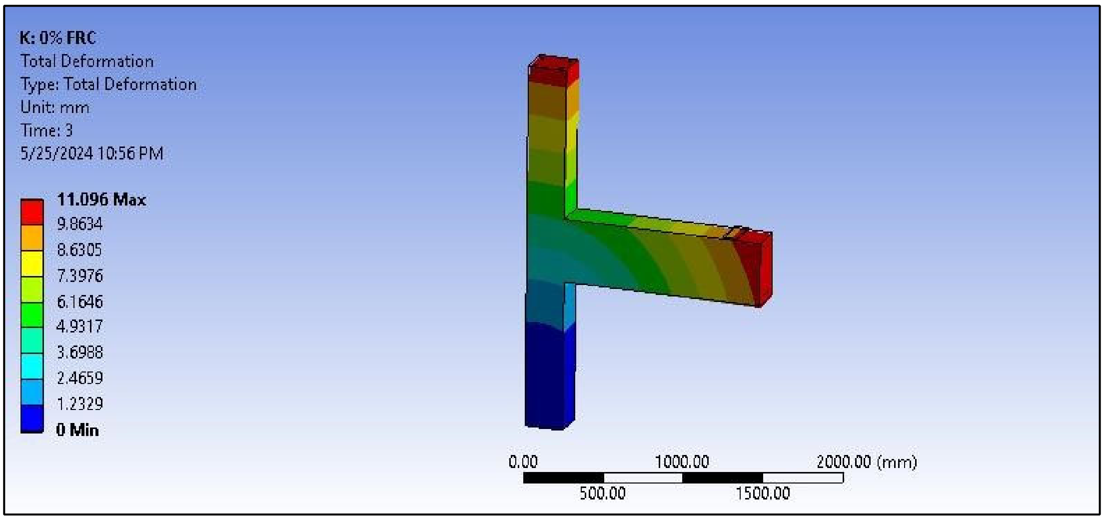

Fig. 8. Deformation at 40 kN load

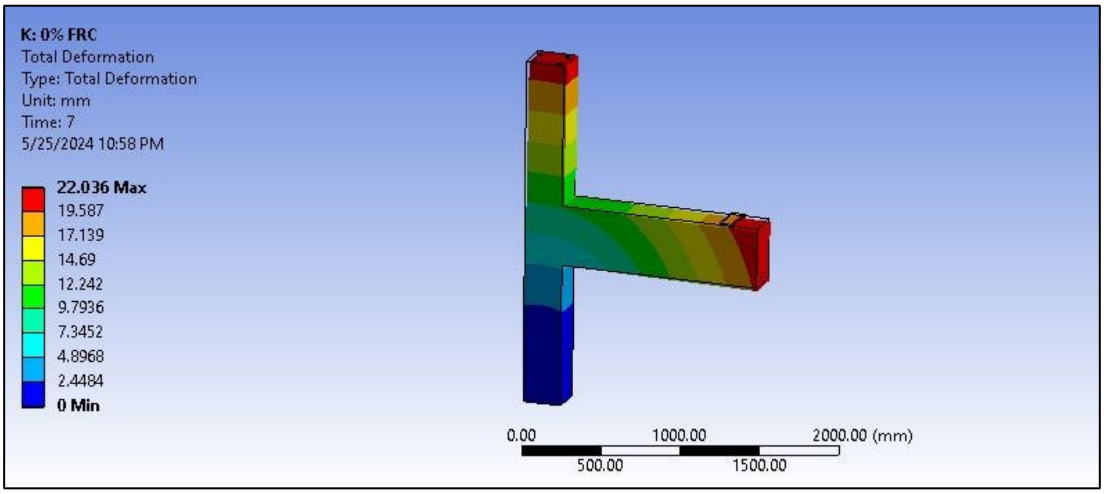

Fig. 9. Deformation at 80 kN load

The deformation plot is obtained for 80 kN load, as shown in Figure 9. The maximum induced deformation on the beam-column joint shows a magnitude of 22.036 mm at the loaded end of the beam. Similarly, the maximum deformation induced on the beam column at 110 kN is shown in Figure 8, which shows a maximum magnitude of 30.24 mm.

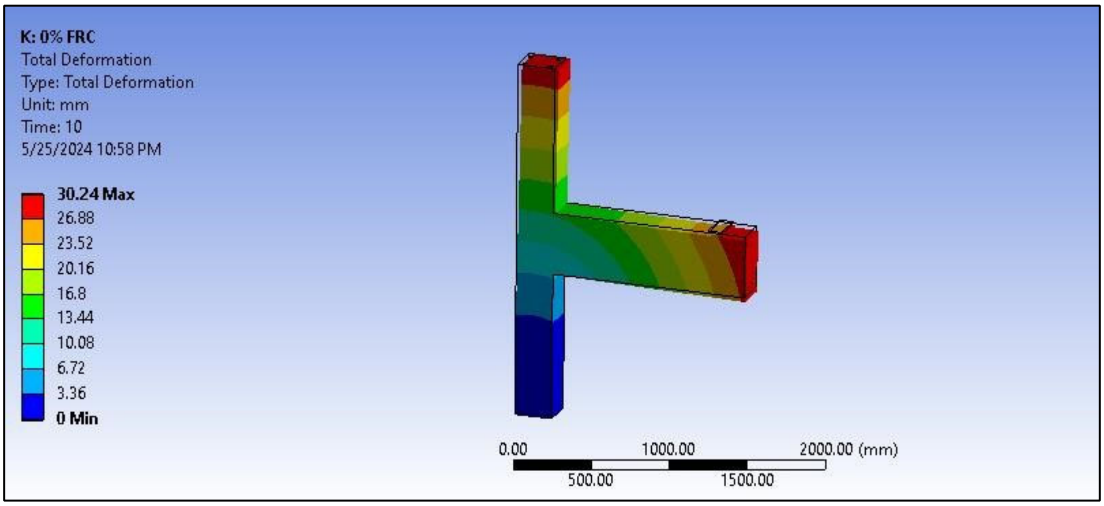

Fig. 10. Deformation at 110 kN load

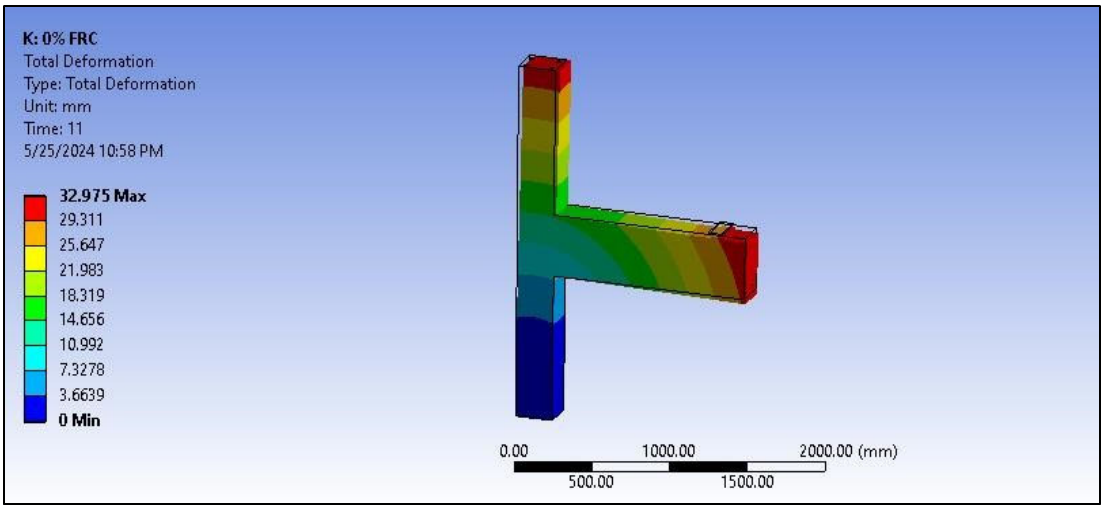

Fig. 11. Deformation at 120 kN load

At 120 kN load, the maximum deformation induced on the structure is 32.975 mm at the free end of the beam where the load is applied, as shown in Figure 11. The deformation is less on the joint, with a magnitude of 10.992 mm.

Shear elastic strain helps assess the elastic behavior of the joint before yielding or damage occurs. Understanding this strain ensures the joint can handle the expected loads without premature failure. Elastic shear strain analysis helps design joints that can absorb and dissipate energy effectively, maintaining structural integrity during and after an earthquake. The elastic shear strain provides insight into how well the joint can transfer loads between the beam and the column without significant deformation, which is crucial for the structure's overall stability. Excessive elastic shear strain can lead to noticeable deflections or vibrations that affect the usability of the building, even if the joint has not reached failure.

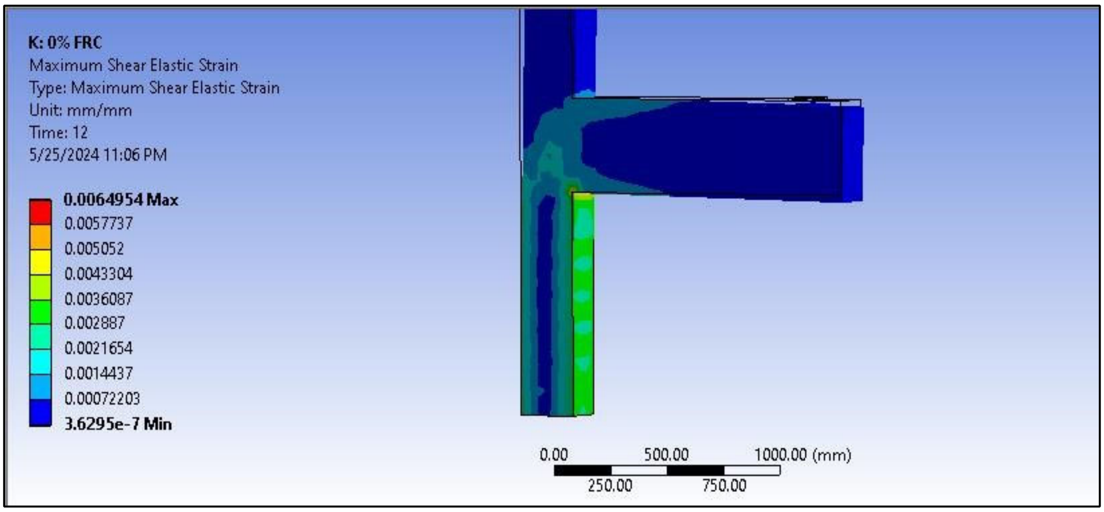

Fig. 12. Maximum shear elastic strain

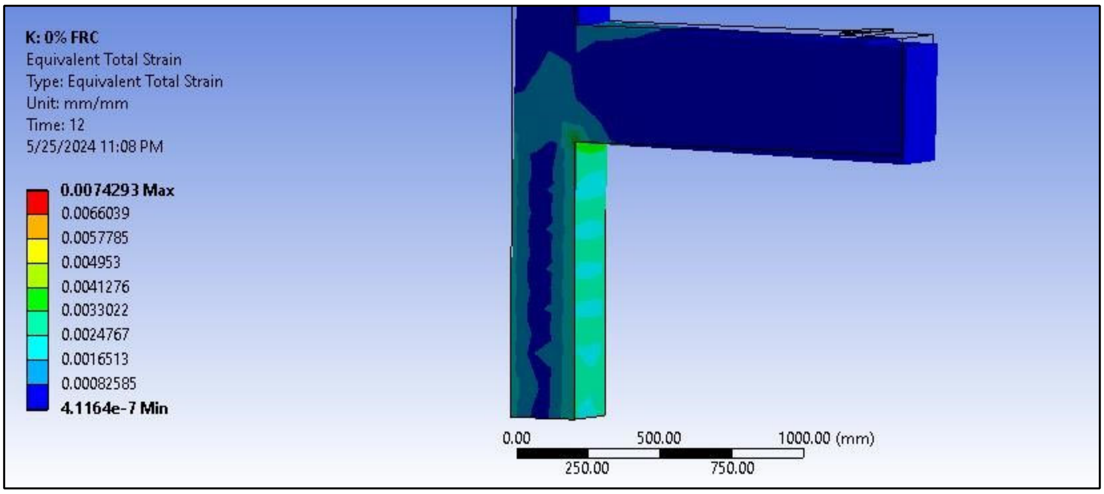

Fig. 13. Maximum equivalent total strain

During seismic events, joints undergo significant shear forces. Understanding shear elastic strain helps design joints that can absorb and dissipate energy, enhancing the structure's ability to withstand earthquakes. The maximum shear elastic strain and equivalent total strain plot is shown in Figure 12 and Figure 13. The maximum shear elastic strain value obtained is 0.00649 mm/mm at the joint, represented by the red-colored zone. The maximum equivalent total strain obtained is 0.007429 mm/mm.

3.4. Structural Analysis using 0.3% FRC Material

The beam-column joint's structural analysis is conducted using 0.3% FRC at different loads. The induced deformation on the beam-column joint at 130 kN load is shown in Figure 14. The maximum deformation magnitude is obtained at the beam end as represented by the red-colored zone, which is nearly 30.163 mm.

The maximum shear elastic strain and equivalent total strain plot are shown in Figure 15 and Figure 16. The maximum shear elastic strain value obtained is 0.00649 mm/mm at the joint, represented by the red-colored zone. The maximum shear elastic strain obtained from the analysis is 0.00538 mm/mm, and the maximum total equivalent elastic strain obtained is 0.00611 mm/mm.

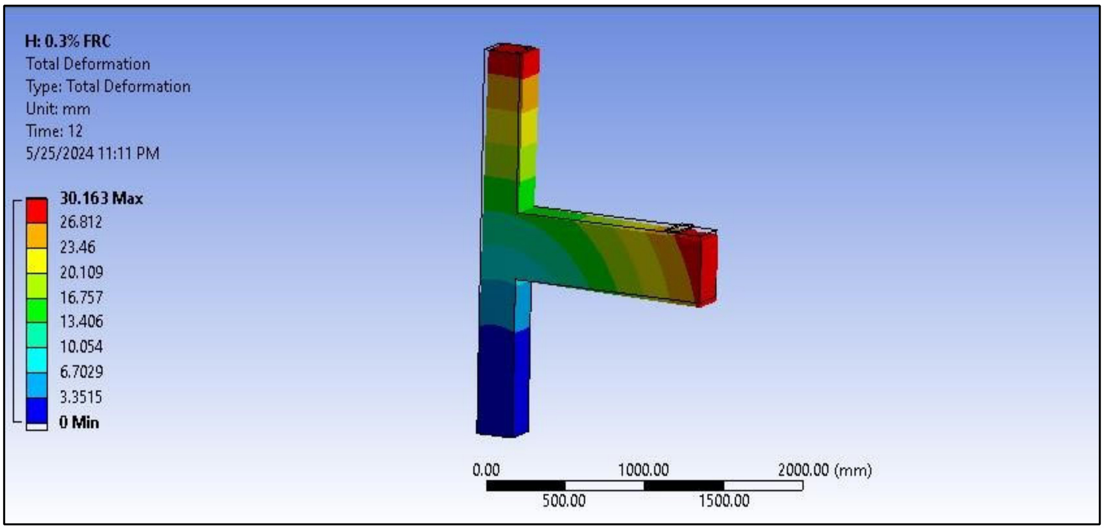

Fig. 14. Total deformation at 130 kN

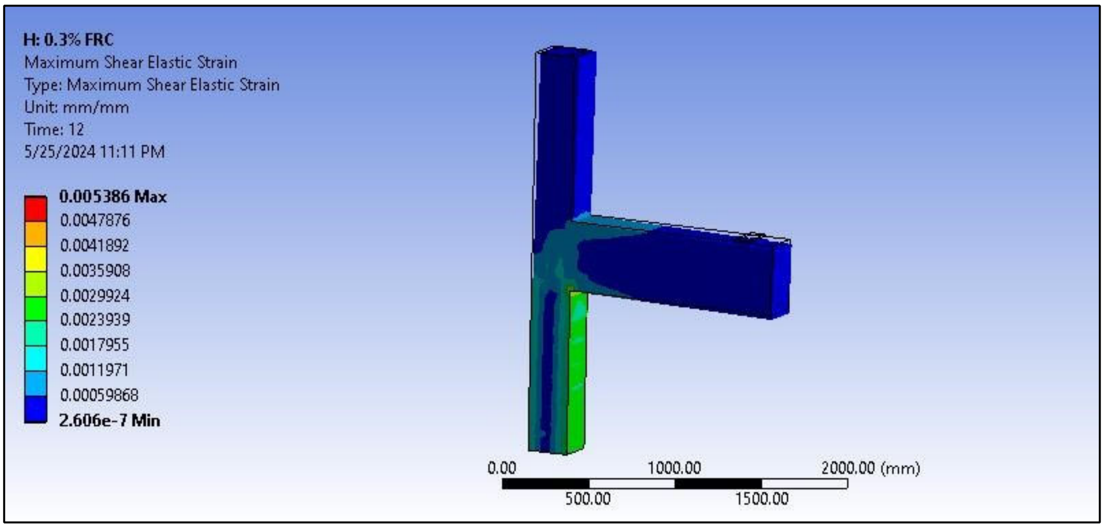

Fig. 15. Maximum shear elastic strain at 130 kN

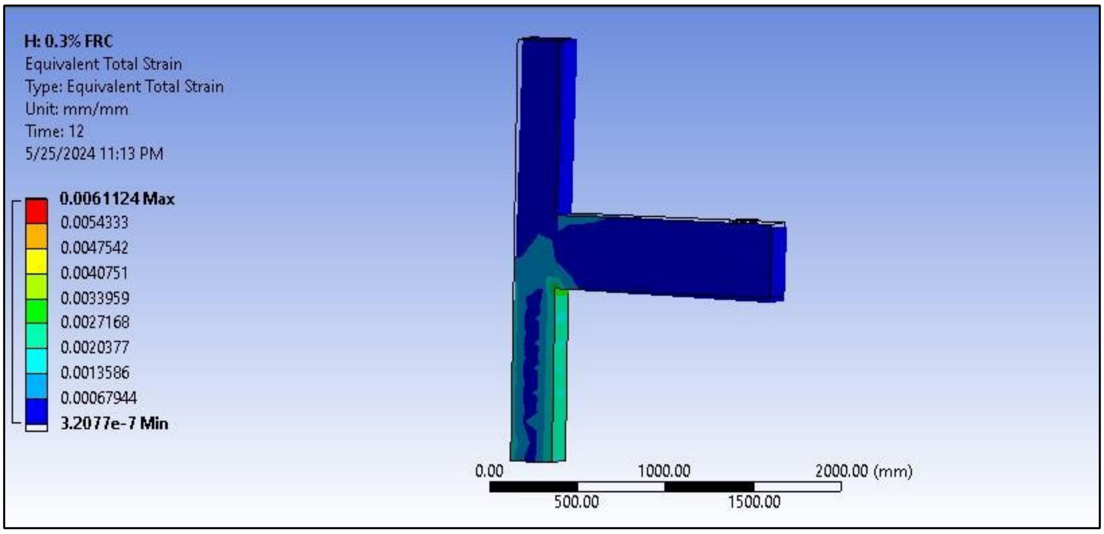

Fig. 16. Equivalent total strain at 130 kN

As per the calculation, the higher strain is obtained at the zone below the beam. These zones include corners, intersections, and at the front base of a bottom portion of a column wherein the magnitude is 0.0020377 mm/mm.

3.5. Structural Analysis using 0.6% FRC Material

The beam-column joint's structural analysis is conducted using 0.6% FRC at different loads. The induced deformation on the beam-column joint at 130 kN load is shown in Figure 17. The maximum deformation magnitude is obtained at the beam end as represented by the red-colored zone, which is nearly 30.021 mm.

The maximum shear elastic strain and equivalent total strain plot are shown in Figure 18 and Figure 19. The maximum shear elastic strain value obtained is 0.00649 mm/mm at the joint, represented by the red-colored zone. The maximum shear elastic strain obtained from the analysis is 0.00535 mm/mm, and the maximum total equivalent elastic strain obtained is 0.006078 mm/mm.

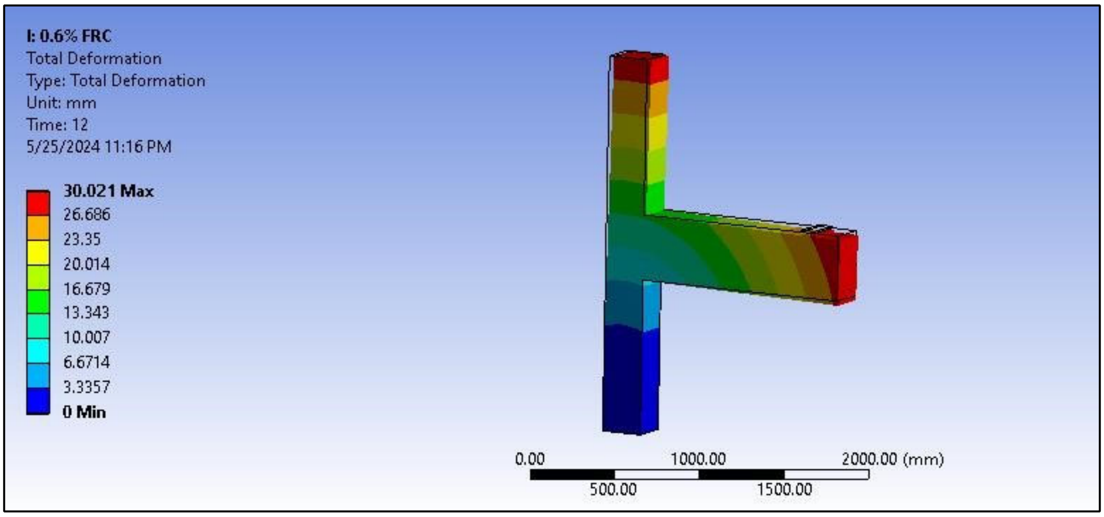

Fig. 17. Total deformation at 130 kN

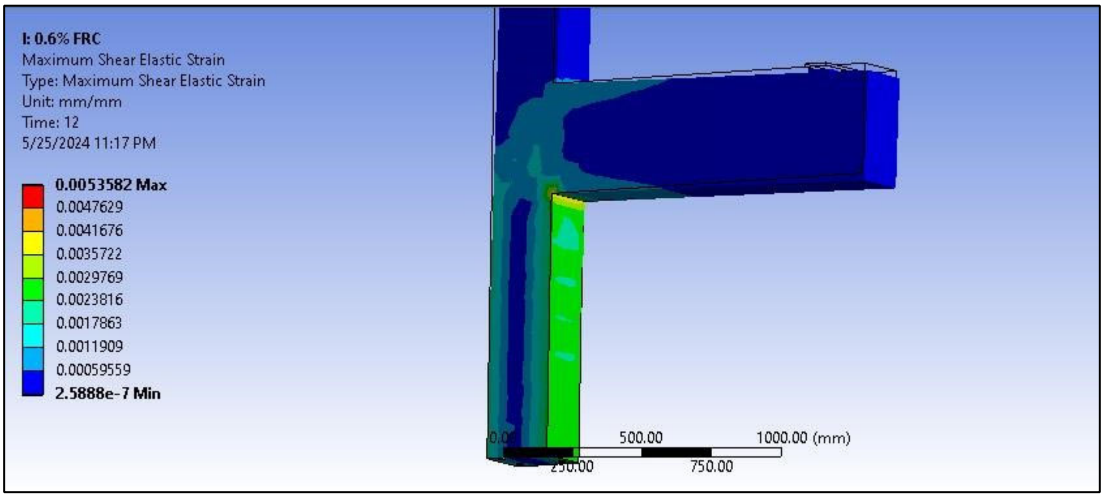

Fig. 18. Maximum shear elastic strain at 130 kN

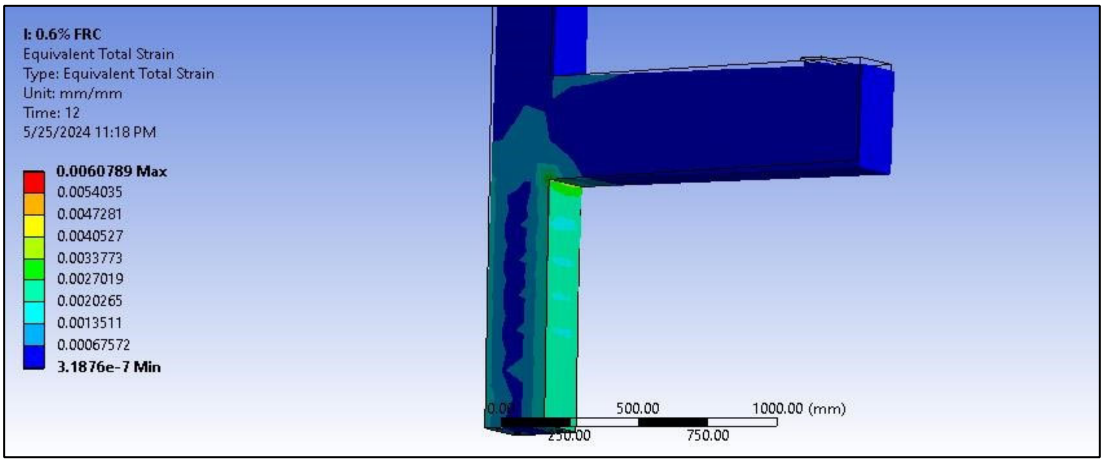

Fig. 19. Equivalent total strain at 130 kN

The higher strain is obtained at the zone below the beam. These zones include corners, intersections, and at the front base of the bottom portion of the column, wherein the magnitude is 0.0020265 mm/mm.

3.6. Structural Analysis using 0.9% FRC Material

The beam-column joint's structural analysis is conducted using 0.9% FRC at different loads. The induced deformation on the beam-column joint at 130 kN load is shown in Figure 20. The maximum deformation magnitude is obtained at the beam end as represented by the red-colored zone, which is nearly 28.762 mm.

The maximum shear elastic strain and equivalent total strain plot are shown in Figure 21 and Figure 22. The maximum shear elastic strain value obtained is 0.00511 mm/mm at the joint, represented by the red-colored zone. The maximum total equivalent elastic strain obtained from the analysis is 0.00578 mm/mm.

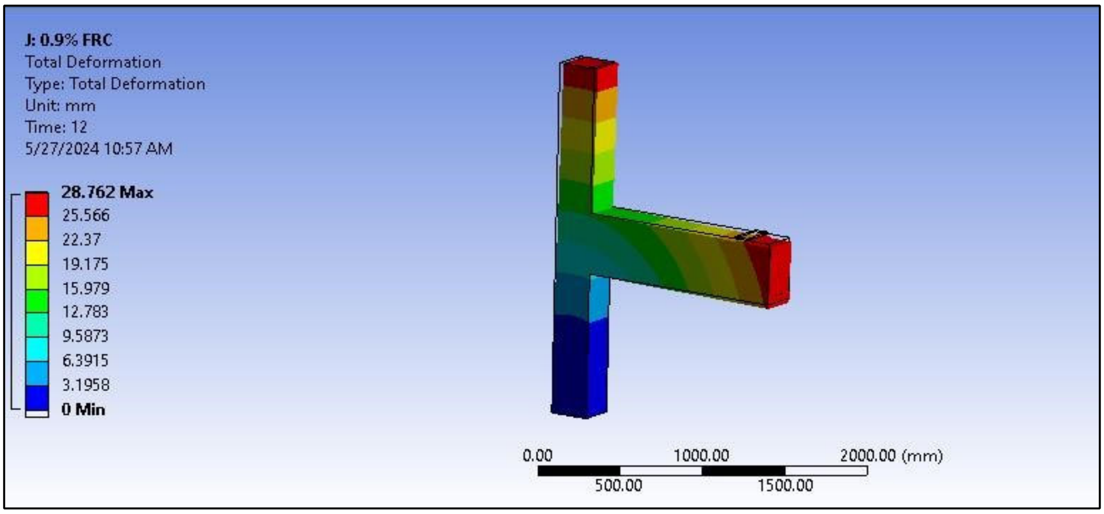

Fig. 20. Total deformation at 130 kN

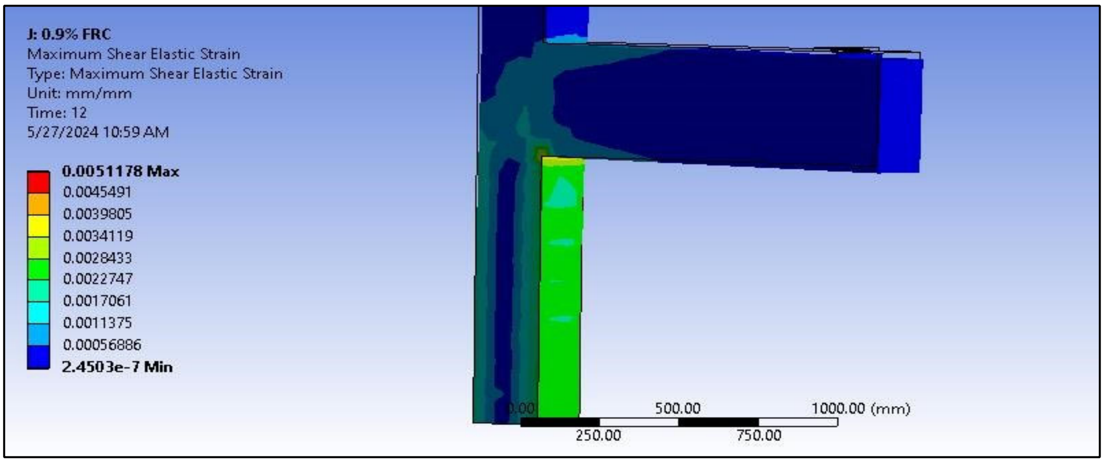

Fig. 21. Maximum shear elastic strain at 130 kN

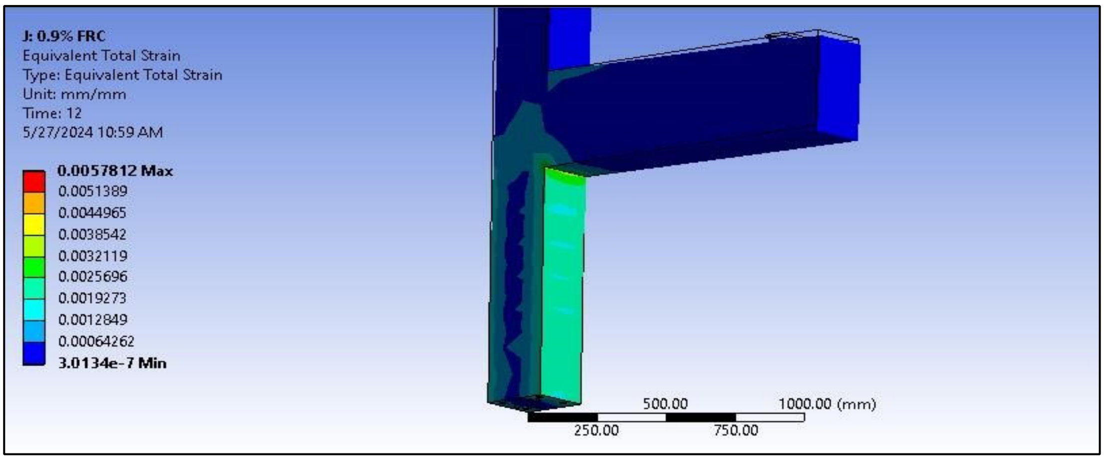

Fig. 22. Equivalent total strain at 130 kN

The higher strain is obtained at the zone below the beam. These zones include corners, intersections, and at the front base of the bottom portion of the column, wherein the magnitude is 0.00192 mm/mm.

4. Comparative Studies

The comparative studies are conducted for different materials, i.e., 0% FRC, 0.3% FRC, 0.6% FRC, and 0.9% FRC, based on deformation, shear elastic strain, and strain energy are shown in Table 2 and expressed in graphical form in Figure 23. The deformation comparison chart is generated at different loads.

Table 2. Deformation comparison data

Load (N)	0% FRC	0.3% FRC	0.6% FRC	0.9% FRC
20000	5.627	4.742	4.719	4.519
30000	8.361	7.052	7.019	6.722
40000	11.096	9.363	9.319	8.926
50000	13.831	11.675	11.620	11.131
60000	16.566	13.986	13.920	13.334
70000	19.301	16.297	16.220	15.538
80000	22.036	18.608	18.520	17.742
90000	24.770	20.919	20.821	19.946
100000	27.505	23.230	23.121	22.150
110000	30.240	25.541	25.421	24.354
120000	32.975	27.852	27.721	26.558
130000	35.710	30.163	30.021	28.762

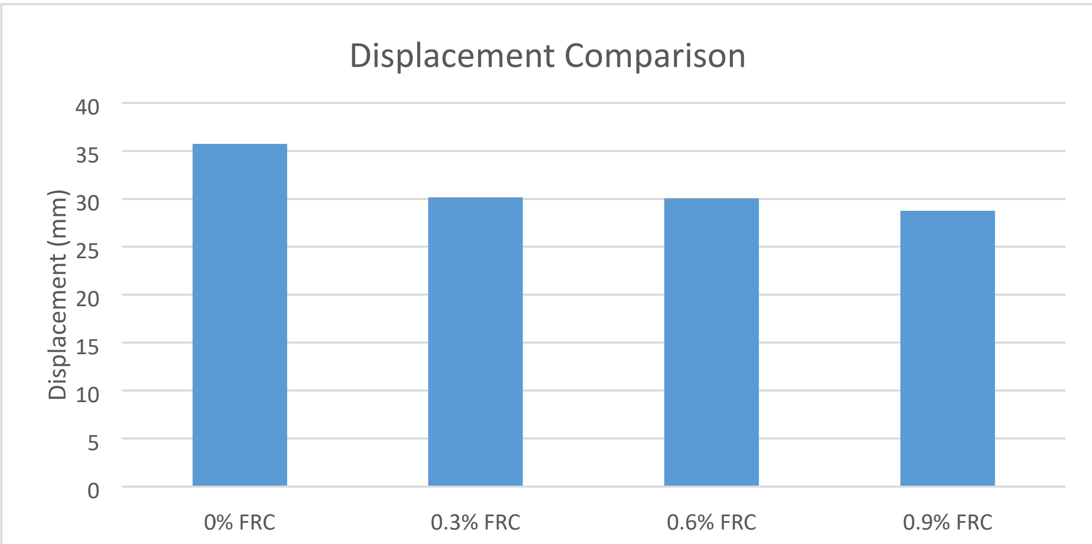

Fig. 23. Displacement comparison plot of FRC's at 130 kN load

At all load levels, the deformations decrease as the FRC concentration increases. This indicates that adding fiber s to the concrete mix enhances the stiffness and reduces the deformation of the beam-column joint under load. The benefits of FRC become more pronounced at higher load levels, i.e., at 130 kN load, the deformation for 0% FRC is 35.71 mm, whereas, for 0.9% FRC, it is 28.762 mm, shown in Tables 3 to 7 and expressed in graphical form in Figure 24, 25 and 26. This indicates a significant improvement in structural performance due to the presence of fibers. Including fibers not only reduces the deformations but also likely improves the beam-column joint's overall durability and crack resistance. The data suggests that FRC effectively enhances the load-carrying capacity and structural integrity. The 0% FRC exhibited the lowest deformation values, indicating the highest stiffness and best performance under load.

Table 3. Shear elastic strain comparison data

Load	0% FRC	0.3% FRC	0.6% FRC	0.9% FRC
20000	0.001246	0.001034	0.001028	0.000980
30000	0.001721	0.001427	0.001420	0.001354
40000	0.002197	0.001822	0.001812	0.001728
50000	0.002674	0.002217	0.002205	0.002103
60000	0.003151	0.002613	0.002599	0.002478
70000	0.003628	0.003009	0.002993	0.002854
80000	0.004106	0.003405	0.003387	0.003229
90000	0.004584	0.003801	0.003781	0.003605
100000	0.005061	0.004197	0.004175	0.003981
110000	0.005539	0.004593	0.004569	0.004357
120000	0.006017	0.004990	0.004963	0.004736
130000	0.006495	0.005386	0.005358	0.005118

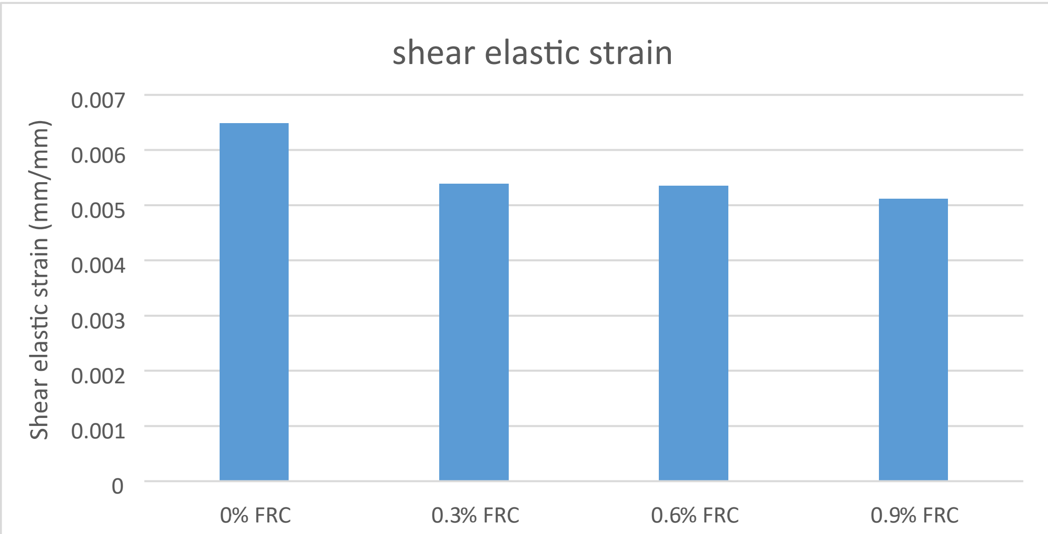

Fig. 24. Shear elastic strain comparison of FRC's at 130 kN load

At a higher load of 130,000 N, the shear strain decreases from 0.0064954 mm/mm for 0% FRC to 0.0051178 mm/mm for 0.9% FRC. The reduction in strain becomes more significant as the load increases, highlighting the fibers contribution to improved performance under higher stresses. Adding fibers to the concrete mix enhances the strength and stability of the beam-column joint. Lower shear strains indicate that the joint can better resist shear forces, improving overall structural integrity. Increased FRC concentration reduces shear stress, allowing the structure to withstand bigger displacements without substantial damage. This improved ductility is critical for constructions subjected to dynamic loads like earthquakes when energy dissipation and deformation capacity are required. At low shear forces, the fibers assist in restricting the spread of reflected microcracks. Improved crack management increases the structure's durability and lifetime. Because shear stress lowers with increasing FRC content, the beam-column connection may support heavier loads without affecting structural integrity. This makes FRC an appealing option for applications requiring high-performance concrete. Stronger and more resilient structures can be produced by incorporating FRC into the design of beam-column connections. The improved shear stiffness and ductility can be utilised by the design to better satisfy performance criteria.

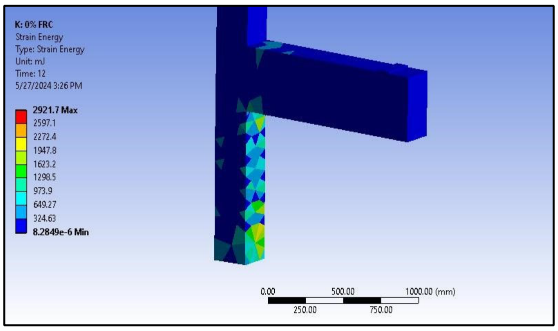

Fig. 25 (a). Strain energy for 0% FRC

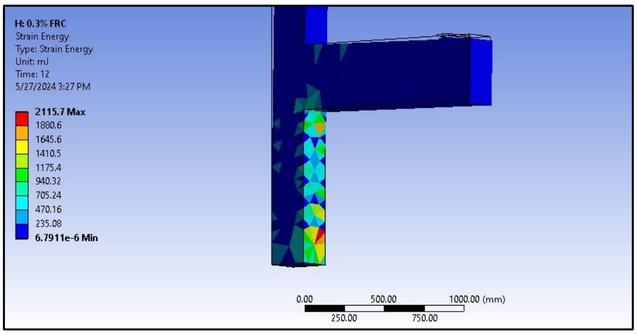

Fig. 25 (b). Strain energy for 0.3% FRC

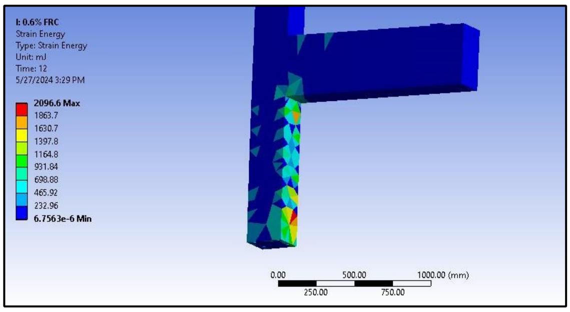

Fig. 25 (c). Strain energy for 0.6% FRC

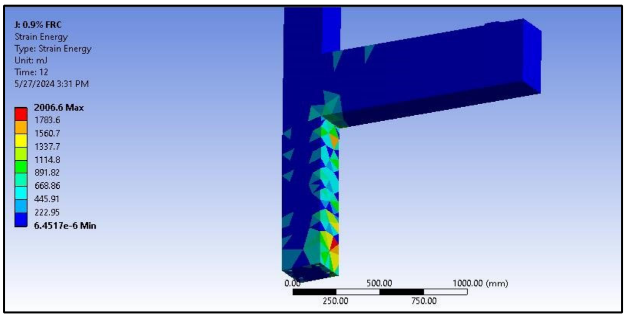

Fig. 25 (d). Strain energy for 0.9% FRC

Table 4. Strain energy comparison data

Load (N)	0% FRC	0.3% FRC	0.6% FRC	0.9% FRC
20000	184.31	131.50	130.26	119.52
30000	296.18	212.23	210.26	193.11
40000	434.46	312.20	309.32	284.28
50000	599.16	431.40	427.45	393.03
60000	791.28	570.38	565.17	519.75
70000	1013.30	731.26	724.60	666.53
80000	1262.80	912.10	903.81	839.14
90000	1539.70	1112.90	1102.80	1032.50
100000	1844.10	1333.70	1321.60	1246.00
110000	2175.90	1574.40	1560.10	1479.50
120000	2535.10	1835.10	1818.50	1733.00
130000	2921.70	2115.70	2096.60	2006.60

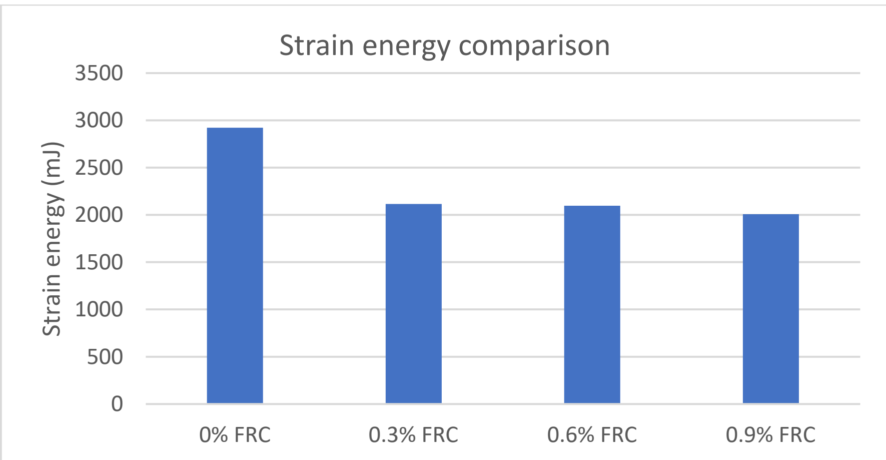

Fig. 26. Strain energy comparison chart of FRC's

At a higher load of 130,000 N, the strain energy drops from 2921.7 for 0% FRC to 2006.6 for 0.9% FRC. The reduction in strain energy becomes more substantial as the strain increases, emphasizing the fiber's role in improving performance at greater strains. Including fibers in the concrete mix improves the strength and stability of the beam-column connection. Lower strain energy suggests the joint can better tolerate applied loads, resulting in greater structural integrity. The strain energy lowers with increasing FRC concentration, enabling the structure to bear larger displacements without significant damage. This increased ductility is essential for buildings subjected to dynamic loads, such as earthquakes, where energy dissipation and deformation capacity are needed. The beam-column connection can handle larger loads without sacrificing structural integrity since the strain energy decreases with increased FRC content. This makes FRC an appealing option for applications requiring high-performance concrete.

Graphene is used in more experiments. Tables 5, 6, and 7 display the strain energy, shear elastic strain, and deformation comparison charts.

Table 5. Deformation comparison chart with graphene

Load (N)	0% FRC	graphene
20000	5.6273	0.16778
30000	8.3617	0.25069
40000	11.096	0.33360
50000	13.831	0.41651
60000	16.566	0.49942
70000	19.301	0.58233
80000	22.036	0.66524
90000	24.770	0.74815
100000	27.505	0.83106
110000	30.240	0.91397
120000	32.975	0.99688
130000	35.710	1.07980

Table 6. Shear elastic strain comparison chart with graphene

Load (N)	0% FRC	graphene
20000	0.001246	6.59E-05
30000	0.001721	9.89E-05
40000	0.002197	0.000132
50000	0.002674	0.000165
60000	0.003151	0.000198
70000	0.003628	0.000231
80000	0.004106	0.000264
90000	0.004584	0.000297
100000	0.005061	0.000330
110000	0.005539	0.000363
120000	0.006017	0.000396
130000	0.006495	0.000429

Table 7. Strain energy comparison chart with graphene

Load (N)	0% FRC	graphene
20000	184.31	4.69
30000	296.18	8.31
40000	434.46	12.97
50000	599.16	18.67
60000	791.28	25.39
70000	1013.30	33.15
80000	1262.80	41.94
90000	1539.70	51.77
100000	1844.10	62.62
110000	2175.90	74.51
120000	2535.10	87.43
130000	2921.70	101.39

Graphene material yields far less deformation at all given loads, as Table 5 demonstrates. Similarly, Table 6 demonstrates that compared to 0% FRC, the shear elastic stress obtained with graphene material is significantly lower.

The strain energy comparison graphic indicates that graphene has far lower values than FRC. Reduced strain energy suggests that the joint has improved energy absorption and dissipation capabilities. This is especially crucial when there is dynamic loading, like during an earthquake, and the structure must be able to bear abrupt and erratic forces (Tafsirojjaman et al. 2021, Webber et al. 2015, Zabihi et al. 2018).

It suggests that the joint distributes stresses more evenly, reducing the likelihood of localized stress concentrations that could lead to cracks or failures. A beam-column joint with lower strain energy can undergo larger deformations without failing. This ductility is crucial for structures that must maintain integrity while experiencing significant displacements. Improved ductility means that after the initial yielding, the joint can still carry loads without catastrophic failure, enhancing the structure's ability to survive extreme events (seismic excitation). Lower strain energy is often associated with higher loadbearing capacity. The joint's ability to withstand larger loads before experiencing critical stress levels increases the structure's overall strength. Less strain energy improves earthquake performance in seismically active areas. The capacity to absorb and disperse seismic energy without inflicting significant damage is essential for structural stability and occupant safety. An assembly is more robust and can better restore to its initial state after being subjected to strong forces if it can sustain high loads with less strain energy.

In other words, the graphene-reinforced joint can handle bigger loads more effectively with less internal energy generated due to the decreased strain energy under greater loads (e.g., 130000 N). This increases the overall bearing capacity of the structure, strengthening and enhancing its dependability. The drop in strain energy indicates increased ductility.

The graphene-reinforced assembly can withstand significant deformation without failing, which is required to maintain structural integrity during intense seismic excitations. Higher ductility also allows the joint to withstand larger displacements, increasing overall stability. The large performance gain with graphene indicates that less material may be required for the same or better structural performance. This can result in cost savings and more effective use of materials in construction projects. The hysteresis data for 0%, 0.3%, 0.6%, and 0.9% FRC are shown in Table 8 and Figure 27.

Table 8. Hysteresis data for 0%, 0.3%, 0.6% and 0.9% FRC

Hysteresis data for							
0% FRC		0.3% FRC		0.6% FRC		0.9% FRC	
Strain (mm/mm)	Stress (MPa)	Strain (mm/mm)	Stress (MPa)	Strain (mm/mm)	Stress (MPa)	Strain (mm/mm)	Stress (MPa)
0	0	0	0	0	0	0	0
1388.3	4.2511E-06	861.7	5.96E-06	640.1	7.99E-06	474.82	1.04E-05
4407.6	0.000005356	2612.2	7.86E-06	1859.4	1.10E-05	1325.9	1.49E-05
8663.4	6.1311E-06	4997.5	9.25E-06	3469.6	1.33E-05	2417.6	1.83E-05
13993	6.7481E-06	7918.7	1.04E-05	5401.2	1.52E-05	3702.3	2.13E-05
20297	7.2692E-06	11316	1.13E-05	7613.5	1.68E-05	5152.8	2.39E-05
27505	7.7247E-06	15149	1.22E-05	10079	1.83E-05	6750.7	2.63E-05
35562	0.000008132	19387	1.30E-05	12776	1.96E-05	8482.6	2.85E-05
44426	8.5021E-06	24005	1.37E-05	15690	2.09E-05	10338	3.05E-05
54062	8.8426E-06	28983	1.44E-05	18807	2.20E-05	12309	3.24E-05
64440	9.1586E-06	34305	1.50E-05	22116	2.31E-05	14388	3.42E-05
61663	6.5651E-07	32581	3.05E-06	20836	7.15E-06	13439	1.35E-05
55624	-1.5534E-06	29080	-7.58E-07	18397	1.12E-06	11737	4.51E-06
47113	-3.1035E-06	24310	-3.53E-06	15177	-3.41E-06	9553.3	-2.44E-06
36453	-4.3376E-06	18468	-5.78E-06	11314	-7.18E-06	6983.8	-8.34E-06
23845	-5.3798E-06	11672	-7.72E-06	6889	-1.05E-05	4082.9	-1.36E-05
9430.4	-6.2907E-06	4005.9	-9.44E-06	1958.8	-1.34E-05	887.04	-1.83E-05
-6683.9	-7.1053E-06	-4469.3	-1.10E-05	-3436.1	-1.61E-05	-2576.8	-2.27E-05
-24412	-7.8456E-06	-13705	-1.24E-05	-9263.4	-1.86E-05	-6287.9	-2.68E-05
-43684	-8.5265E-06	-23661	-1.37E-05	-15497	-2.09E-05	-10230	-3.06E-05
-64440	-9.1586E-06	-34305	-1.50E-05	-22116	-2.31E-05	-14388	-3.42E-05
-61663	-6.5651E-07	-32581	-3.05E-06	-20836	-7.15E-06	-13439	-1.35E-05
-55624	1.5534E-06	-29080	7.58E-07	-18397	-1.12E-06	-11737	-4.51E-06
-47113	3.1035E-06	-24310	3.53E-06	-15177	3.41E-06	-9553.3	2.44E-06
-36453	4.3376E-06	-18468	5.78E-06	-11314	7.18E-06	-6983.8	8.34E-06
-23845	5.3798E-06	-11672	7.72E-06	-6889	1.05E-05	-4082.9	1.36E-05
-9430.4	6.2907E-06	-4005.9	9.44E-06	-1958.8	1.34E-05	-887.04	1.83E-05
6683.9	7.1053E-06	4469.3	1.10E-05	3436.1	1.61E-05	2576.8	2.27E-05
24412	7.8456E-06	13705	1.24E-05	9263.4	1.86E-05	6287.9	2.68E-05
43684	8.5265E-06	23661	1.37E-05	15497	2.09E-05	10230	3.06E-05
64440	9.1586E-06	34305	1.50E-05	22116	2.31E-05	14388	3.42E-05

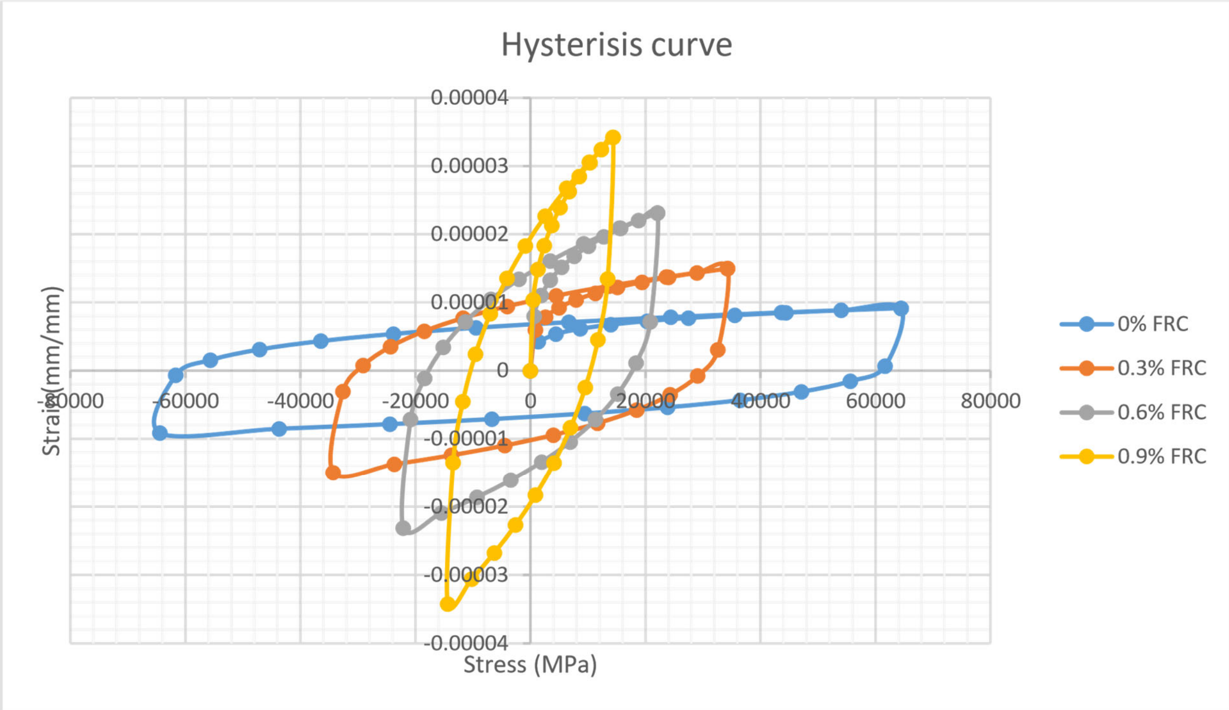

Fig. 27. Hysteresis comparison chart

Hysteresis loops indicate the material's energy dissipation capacity. For 0% FRC, the initial hardness is obvious, but the energy loss lowers significantly as the strain grows, indicating poor ductility and absorption. The introduction of FRC widens the hysteresis loops, particularly at higher concentrations (0.6 and 0.9%), indicating enhanced energy dissipation and ductility.

The stress in 0% FRC initially climbs but then decreases significantly as the strain increases, showing a lack of material recovery and considerable plastic deformation.

0.3% FRC improves stress levels for similar strain values compared to 0% FRC, showing improved stiffness and energy dissipation.

The stress level improves with 0.6% FRC, demonstrating that increasing FRC content correlates to increased bearing capacity and stiffness.

0.9% FRC has the highest stress levels for given load values and performs best in terms of hardness, energy absorption, and ductility.

As the FRC concentration increases, the material's hardness degrades less during cyclic stress. Higher FRC content (0.6% and 0.9%) reduces stress after numerous cycles while improving fatigue resistance and durability.

0% FRC shows low ductility and a considerable stress reduction following initial strain. 0.3% and 0.6% FRC exhibit increased ductility when greater stress levels are sustained at higher loads. 0.9% FRC demonstrates the highest ductility by bearing higher stress across the whole load range, indicating that it can withstand larger deformations without failure. The degradation of hardness is less pronounced at higher FRC concentrations.

0.9% FRC exhibits the least hardness degradation by retaining greater stress levels in overall loading ranges, showing that the material retains structural integrity over multiple loading cycles. Structures with high FRC content, particularly 0.6% and 0.9%, are better suited to seismic zones due to higher energy dissipation, ductility, and less stiffness loss. The ductility and stiffness for various FRC are shown in Tables 9 and 10.

Table 9. Ductility comparison chart at fracture

Fiber Concentration	Ductility (mm/mm)	Percentage Enhancement
0% FRC	6683.9	Reference*
0.3% FRC	28983	2.087%
0.6% FRC	22116	1.594%
0.9% FRC	14388	1.039%

* – Because we assumed the 0% FRC ductility as the base or neutral point or reference point for doing the work

Table 10. Stiffness comparison chart

Fiber Concentration	Stiffness (MPa)	Percentage Enhancement
0% FRC	36152	100%
0.3% FRC	38901	7.6%
0.6% FRC	41611	15.1%
0.9% FRC	44518	22.1%

Higher FRC concentrations can reduce material consumption while boosting load capacity and structure longevity. This can result in more cost-effective designs with higher performance. Hysteresis results clearly show that raising the FRC concentration in beam-column connections increases energy dissipation, ductility, stiffness, and overall structural integrity. In particular, 0.6% and 0.9% FRC concentrations work best, making them ideal for applications that require great durability and flexibility under cyclic loading circumstances (Zi-wei et al. 2021).

The area of the hysteresis loop signifies the energy expended during cyclic loading. At 0% FRC, the area is minimal, indicating reduced energy dissipation and damping efficacy, as illustrated in Figure 28. The gradient of the unloading and loading curves denotes stiffness. The hardness of 0% FRC markedly diminishes with escalating load, indicating degradation under cyclic stress. Its narrow hysteresis loop and reduced strain range constrain the material's ductility.

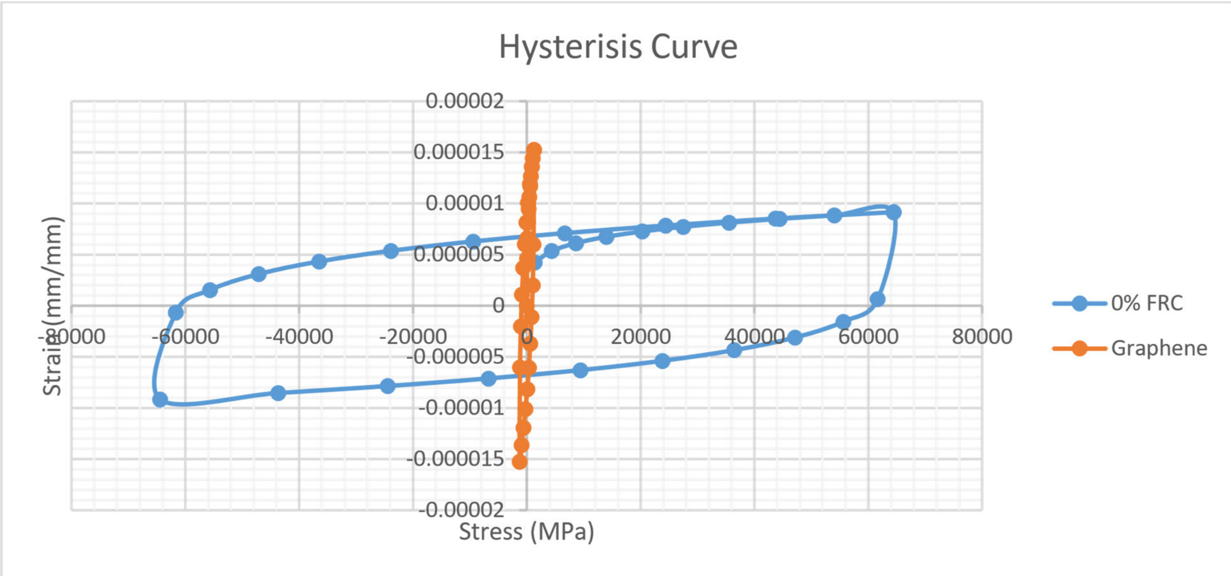

Fig. 28. Hysteresis curve for FRC and graphene

Concrete reinforced with graphene has improved damping and energy dissipation capabilities, making it ideal for buildings subjected to dynamic loads like earthquakes. Concrete reinforced with graphene shows less loss in stiffness as load increases. This suggests that adding graphene to concrete improves its capacity to retain rigidity. The hysteresis loop is longer for reinforced graphene concrete, indicating increased ductility. This means that the material can withstanding larger deformations without distortion, which is important for seismic performance.

While both materials are quite stiff initially, concrete reinforced with graphene stays stiff when loads are higher. Compared to zero fiber-reinforced concrete, graphene-reinforced concrete exhibits larger peak stresses at lower strains, indicating improved strength.

In concrete reinforced with graphene, residual stress (permanent deformation after unloading) is reduced, indicating improved shape recovery and reduced long-term damage. Concrete reinforced with graphene shows higher peak stress levels after cyclic loading, indicating improved load capacity. Because graphene has better energy dissipation and ductility than other materials, it is more appropriate for seismic applications in concrete. Because of its increased efficiency in absorbing and releasing energy, there is a decreased chance of a catastrophic failure during an earthquake.

The reduced stiffness deterioration and improved strength retention suggest that concrete reinforced with graphene can sustain structural integrity over long periods, even when subjected to cyclic loads. Adding graphene to concrete can result in beam-column configurations that are more flexible and durable. Engineers can lower construction and material costs by using lighter materials while maintaining strength.

Compared to zero fiber-reinforced concrete, graphene-reinforced concrete achieves maximum stress levels at higher strains, resulting in improved performance under higher loads. Following unloading in graphene-reinforced concrete, superior load recovery results in reduced permanent deformation and improved structural integrity over time.

Fiber-reinforced concrete's mechanical qualities, such as strength, ductility, and energy dissipation capacity, are greatly improved by adding graphene. Graphene-reinforced concrete is a viable alternative for crucial structural elements like beam-column connections, particularly in seismic zones. Improved cycle performance increases suppleness and robustness, resulting in stronger, safer structures.

5. Conclusion

Elevated FRC concentrations can be used to increase structural durability and load capacity while using less material. This could result in more performance-enhancing and cost-effective designs. Studies show that increasing the fraction of reinforced concrete (FRC) in beam-column joints improves the joints' energy dissipation, ductility, stiffness, and overall structural integrity. In particular, FRC concentrations between 0.6% and 0.9% work well, making them appropriate for applications where great durability and flexibility are required under cyclic stress conditions.

1. Incorporating 0.3% FRC enhanced the ductility of beam-column connections by 2087%, leading to a substantial improvement in deformation and energy dissipation capacity.
2. 0.6% FRC enhanced the ductility of beam-column connections by 1594% over 0% FRC. 0.9% FRC increased the ductility of the beam-column connection by 1039% over 0% FRC.
3. The higher ductility of the beam-column joint significantly increases the joint's ability to undergo large deformations and redistribution of loads. This enhances the ductile behavior of the beam-column joint and its resistance to brittle behavior. This makes it highly beneficial in seismic-prone zones, where structures must withstand significant deformation demands while maintaining structural integrity.
4. The deformation induced with graphene fiber is nearly 33 times less than that induced with 0% FRC concrete, which shows graphene's good lateral load-resisting behavior.
5. The strain energy induced with graphene fiber is nearly 28.8 times less than that induced with 0% FRC concrete. Reducing strain energy leads to improved stability, ductility, fracture toughness, lateral load resistance, and seismic resistance, which justifies its suitability to earthquake-prone regions.
6. The incorporation of 0.3% FRC has shown stiffness enhancement of 7.6% compared to 0% FRC.
7. Incorporating 0.6% FRC has shown stiffness enhancement of 7.6% compared to 0% FRC. The findings suggest a slight increase in the material's rigidity and ability to withstand applied forces with less deformation. The incorporation of fibers contributes to a more resilient and durable structural system.
8. The incorporation of 0.6% FRC has shown stiffness enhancement of 15.1% as compared to 0% FRC.
9. The incorporation of 0.6% FRC has shown stiffness enhancement of 22.1% as compared to 0% FRC.

After initial deformation, 0% FRC shows a large reduction in stress and minimal ductility. Greater stress levels and greater ductility are observed at 0.3% and 0.6% concentrations of FRC. By withstanding increased stress over the complete stress spectrum, 0.9% FRC demonstrates better ductility and demonstrates its ability to withstand large deformations without failing. The hardness decreases less noticeably as the FRC concentration increases.

As load increases, concrete reinforced with graphene shows less loss of its rigidity. This suggests that adding graphene to concrete improves its capacity to retain rigidity. The concrete exhibits a larger and more ductile hysteresis loop with graphene reinforcement. This means the material can withstand larger deformations before failing, which is crucial for seismic performance.

Concrete reinforced with graphene has improved energy dissipation and ductility, making it more suitable for earthquake applications. Because of its increased efficiency in absorbing and releasing energy, there is a decreased chance of a catastrophic failure during an earthquake. More resilient and long-lasting beam-column connections may result from incorporating graphene into concrete. Engineers can decrease costs associated with materials and construction by designing stronger, lighter structures.

The authors extend their appreciation to the Deanship of Research and Scientific Studies at King Khalid University for funding this work through large group Research Project under grant number RGP2/306/45

References

Alavi-Dehkordi, S., Mostofinejad, D., & Alaee, P. (2019). Effects of high-strength reinforcing bars and concrete on seismic behaviour of RC beam-column joints, *Eng. Struct.*, *183*, 702-719. ttps://doi.org/10.1016/J.ENGSTRUCT.2019.01.019

Algassem, O., & Vollum, R.L. (2023). Behaviour and design of monotonically loaded reinforced concrete external beam-column joints. *Structures*, *52*, 946-970.

Al-Mahmoud, F., Shaikh, F.U.A., & Maalej, M. (2020). Graphene oxide-impregnated carbon fibres and their impact on the mechanical and durability properties of cementitious composites. *Materials & Design*, *188*, 108412.

Batalha, N., Rodrigues, H., Arede, A., Furtado, A., Sousa, R., & Varum, H. (2022). Cyclic behaviour of precast beam-to-column connections with low seismic detailing. *Earthq Engineering Struct. Dyn.*, *51*(5), 1096-114. https://doi.org/10.1002/eqe.3606

Behnam, H., Kuang, J.S., Huang, R.Y.C. (2017). Exterior RC wide beam-column connections: effect of beam width ratio on seismic behaviour, *Eng. Struct.*, *147*, 27-44. https://doi.org/10.1016/J.ENGSTRUCT.2017.05.044

Cimmino, M., Magliulo, G., & Manfredi, G. (2020). Seismic collapse assessment of new European single story RC precast buildings with weak connections. *Bull Earthq. Eng.*, *18*(15), 6661-86. https://doi.org/10.1007/s10518-020-00952-7

Dang, C.T., & Dinh, N.H. (2017). Experimental study on structural performance of RC exterior beam column joints retrofitted by steel jacketing and haunch element under cyclic loading simulating earthquake excitation. *Adv. Civ. Eng.* https://doi.org/10.1155/2017/9263460

del Vecchio, C., di Ludovico, M., Prota, A., & Manfredi, G. (2015). Analytical model and design approach for FRP strengthening of non-conforming RC corner beam–column joints. *Engineering Struct*ure, *87*, 8-20, https://doi.org/10.1016/J.ENGSTRUCT.2015.01.013

del Vecchio, C., di Ludovico, M., Prota, A., & Manfredi, G. (2016). Modelling beam-column joints and FRP strengthening in the seismic performance assessment of RC existing frames. *Composite Structure*, *142*, 107-116, https://doi.org/10.1016/J.COMPSTRUCT.2016.01.077

Dimov, D., Amit, I., Gorrie, O., Barnes, M.D., Withers, F., Russo, S., & Craciun, M.F. (2018). Ultrahigh Performance Nano engineered Graphene-Concrete Composites for Multifunctional Applications. *Advanced Functional Materials*, *28*(23), 1705183.

Ghayeb, H.H., Razak, H.A., & Sulong, N.H.R. (2017). Development and testing of hybrid precast concrete beam-to-column connections under cyclic loading. *Constr. Build. Mater.*, *151*, 258-278.

Ghayeb, H.H., Razak, H.A., & Sulong, N.R. (2020). Performance of dowel beam-to-column connections for precast concrete systems under seismic loads: a review. *Constr. Build Mater*, *237*, 117582. https://doi.org/10.1016/j.conbuildmat.2019.117582

Guan, D.Z., Guo, Z.X., Xiao, Q.D., & Zheng, Y.F. (2016). Experimental study of a new beam to column connection for precast concrete frames under reversal cyclic loading. *Adv. Struct. Eng.*, *19*(3), 529-545.

Ilia, E., & Mostofinejad, D. (2019). Seismic retrofit of reinforced concrete strong beam–weak column joints using EBROG method combined with CFRP anchorage system. *Eng. Struct*., *194*, 300-319. https://doi.org/10.1016/J.ENGSTRUCT.2019.05.070

Isha, Verma, & Setia, S. (2019). Seismic Behaviour of Stiffened Steel Plate Shear Walls, *International Journal of Innovative Technology and Exploring Engineering (IJITEE)*, *8*(8).

Isha, Verma, Parveen, Berwal, Saraswati, Setia, et al. (2020). Analysis on the Behaviour of Stiffened and unstiffened steel plate shear wall with enhanced performance. International Symposium on Fusion of Science and Technology (ISFT), *IOP Conf. Series: Materials Science and Engineering*, *804*, 012035, IOP Publishing. https://doi.org/10.1088/1757899X/804/1/012035

Jian-Qiang, H., & Yang, L. (2013). Beams and column's connected forms of unbonded precast concrete frame structure, measuring technology and mechatronics, in: Automation (ICMTMA), *Fifth International Conference on, IEEE*, pp. 338-340.

Khan, M.I., Al-Osta, M.A., Ahmad, S. & Rahman, M.K. (2018). Seismic behaviour of beam column joints strengthened with ultra-high performance fibre reinforced concrete. *Compos. Struct.*, *200*, 103-119. https://doi.org/10.1016/j.compstruct.2018.05.080

Kosior-Kazberuka, M., & Berkowski, P. (2016). Fracture Mechanics Parameters of Fine-Grained Concrete with Polypropylene Fibres. *World Multidisciplinary Civil Engineering-Architecture-Urban Planning Symposium*, WMCAUS 2016.

Kremmyda, G.D., Fahjan, Y.M., Psycharis, I.N., & Tsoukantas, S.G. (2017). Numerical investigation of the resistance of precast RC pinned beam-to-column connections under shear loading. *Earthquake Engineering Structure Dyn.*, *46*(9), 1511-29. https://doi.org/10.1002/eqe.2868

Magliulo, G., Cimmino, M., Ercolino, M., Manfredi, G., (2017). Cyclic shear tests on RC precast beam to-column connections retrofitted with a three-hinged steel device. *Bull Earthquake Engineering*, *15*(9), 3797-817. https://doi.org/10.1007/s10518-017-0114-x

Megget, L.M. (2003). The seismic design and performance of reinforced concrete beam column knee joints in buildings, *Earthquake Spectra*, *19*(4), 863-895.

Parra-Montesinos, G.J., Dasgupta, P., & Goel, S.C. (2005). Development of connections between hybrid steel truss–FRC beams and RC columns for precast earthquake-resistant framed construction, *Eng. Struct.*, *27*(13), 1931-1941.

Parveen, Berwal, et al. (2023). Energy Efficient Resource Allocation in Cloud Environment using Metaheuristic Algorithm. *IEEE Access*, *11*, 126135-126146. https://doi.org/10.1109/ACCESS.2023.3330434

Parveen, Berwal, Nakul, Gupta, Ravi, Kumar, et al. (2024). Environmental Conservation by Using Recycled Aggregates: Enhancing Sustainability in Road Construction. *Rocznik Ochrona Środowiska*, *26*, 510-524. https://doi.org/10.54740/ros.2024.047

Realfonzo, R., Napoli, A., Pinilla, J.G.R. (2014). Cyclic behaviour of RC beam-column joints strengthened with FRP systems. *Construction Building Material*, *54*, 282-297. https://doi.org/10.1016/j.conbuildmat.2013.12.043

Santarsiero, G. & Masi, A. (2015). Seismic performance of RC beam-column joints retrofitted with steel dissipation jackets. *Engineering Structures*, *85*, 95-106.

Sharma, R., & Bansal, P.P. (2019). Behavior of RC exterior beam column joint retrofitted using UHP-HFRC, *Construct. Build. Mater.*, *195*, 376-389, https://doi.org/10.1016/j.conbuildmat.2018.11.052

Tafsirojjaman, T., Fawzia, S., Thambiratnam, D., & Zhao, XL. (2021). FRP strengthened SHS beam-column connection under monotonic and large-deformation cyclic loading. *Thin-Walled Struct*, *161*, 107518. https://doi.org/10.1016/j.tws.2021.107518

Wahjudi, D.I., Suprobo, P., & Sugihardjo, H. (2014). Behaviour of precast concrete beam to-column connection with U- and L-bent bar anchorages placed outside the column panel-analytical study. *Procedia Eng.*, *95*, 112-121.

Wang, B., Zhu, S., Xu, Y.L., Jiang, H. (2018). Seismic retrofitting of non-seismically designed RC beam-column joints using buckling-restrained haunches: design and analysis, *Journal of Earthquake Eng.*, *22*, 1188-1208. https://doi.org/10.1080/13632469.2016.1277441

Wang, G.L., Dai, J.G., & Bai, Y.L. (2019). Seismic retrofit of exterior RC beam-column joints with bonded CFRP reinforcement: an experimental study, *Compos. Struct.*, *224*, 111018. https://doi.org/10.1016/J.COMPSTRUCT.2019.111018

Wang, H., Barbagallo, F., & Pan, P. (2020). Test of precast pre-stressed beam-to-column joint with damage-free reinforced concrete slab, *Eng. Struct*., *210*, 110368, https://doi.org/10.1016/j.engstruct.2020.110368

Waqas, H.A., Sahil, M., Khan, M.M., & Hasnain, M. (2023). Predictive model for load-carrying capacity of reinforced concrete beam–column joints using gene expression programming. *Proceedings of the ASEC 2023, MDPI, Basel Switzerland*, p. 67.

Waqas, H.A., Sahil, M., Khan, M.M., Anwar, A.W., Shah, M.U., & Usman, M. (2024). Optimizing reinforcement strategies for robust beam-column joints in seismic-resistant structures. *Arabian J. Sci. Eng.* https://doi.org/10.1007/s13369-023-08591-1

Webber, A, Orr, J.J., Shepherd, P., & Crothers, K. (2015). The effective length of columns in multistorey frames. *Engineering Structure*, *102*, 132-43. https://doi.org/10.1016/j. engstruct.2015.07.039

Zabihi, H.H., Tsang, E.F. & Gad, J.L. (2018). Wilson, Seismic retrofit of exterior RC beam column joint using diagonal haunch, *Engineering Structure*, *174*, 753-767. https://doi.org/10.1016/J.ENGSTRUCT.2018.07.100

Zi-wei, Cai, Xin, Liu, Ling-zhi, Li, Zhou-dao, Lu, & Yu, Chen, (2021). Seismic performance of RC beam column slab joints strengthened with steel haunch system, *J. Build. Eng.*, *44*. https://doi.org/10.1016/j.jobe.2021.103250

Zoubek, B., Isakovic, T., Fahjan, Y., & Fischinger, M. (2013). Cyclic failure analysis of the beam-to-column dowel connections in precast industrial buildings. *Eng. Struct.*, *52*, 179-191.